Research Article ISSN 2639-9458

Microbiology & Infectious Diseases

Pharmacophore Investigations of Potential COVID-19 RNA Polymerase(RdRp) Inhibitors: Repurposing FDA-Approved Drugs

Valentina L. Kouznetsova[1,5], Caroline Kellogg[2], Aidan Zhang[2,3], Mahidhar Tatineni[1], Mark A. Miller[1] and Igor F. Tsigelny[1,4,5*]

[1]*San Diego Supercomputer Center, UC San Diego, Calif.*

[2]*REHS program, San Diego Supercomputer Center, UC San Diego, Calif.*

[3]*MAP program, San Diego Supercomputer Center, UC San Diego, Calif.*

[4]*Dept. of Neurosciences, UC San Diego, Calif.*

[5]*BiAna, San Diego, Calif.*

***Correspondence:**
Igor F. Tsigelny, Dept. of Neurosciences, San Diego Supercomputer Center, UC San Diego, Calif.

Received: 30 December 2020; **Accepted:** 27 January 2021

Citation: Kouznetsova VL, Kellogg C, Zhang A, et al. Pharmacophore investigations of potential Covid-19 RNA polymerase(RdRp) inhibitors: Repurposing FDA-approved drugs. Microbiol Infect Dis. 2021; 5(1): 1-9.

ABSTRACT

Background: *SARS-CoV-2 has caused tens of millions of infections worldwide and millions of deaths. Currently, no effective treatment has been identified against the virus. Of its viral proteins, the RNA-dependent RNA polymerase (RdRp) is a promising target for drug design because of its importance in the replication of the virus.*

Material and Methods: *After the identification of an RdRp pocket site based on the crystal structure of the RdRp–nsp7–nsp8 complex and the triphosphate form of remdesivir (PDB ID: 7BV2), we created a pharmacophore model consisting of 11 different features. These features include two acceptors, three donors, one acceptor and donor, three donor or acceptor, and one hydrophobic; an excluded volume of R=1.1 Å was also added. We then ran a pharmacophore search on our conformational database (DB) of approximately 2500 FDA-approved drugs and 600 000 conformations to identify potential drug-candidates. To determine the drugs that bound the best, we conducted multi conformational docking of these results to the previously identified pocket site.*

Results: *The pharmacophore search found 315 different potential inhibitors of RdRp, of which 85 were chosen based on the number of H-bonds and hydrophobic interactions in the best docking pose. Several of the drugs selected, including ritonavir, dasatinib, imatinib, and sofosbuvir, have previously been shown to be effective against other viruses.*

Conclusions: *These findings highlight compounds that could lead to both in vitro and in vivo studies to identify potential treatments against SARS-CoV-2.*

Keywords
COVID-19, FDA-Approved Drugs, Virus, Pharmacophore

Introduction
Coronaviruses are a family of viruses associated mostly with respiratory disease in a variety of animal species and humans. In particular, severe acute respiratory syndrome virus (SARS-CoV), Middle East respiratory syndrome virus (MERS-CoV), and the recently emerged SARS-CoV-2 virus have all been responsible for global outbreaks. SARS-CoV-2 remains a large threat to public health today, with over 95.4 million cases and 2.03 million deaths confirmed worldwide as of January 18, 2021 [1]. Other less pathogenic human coronaviruses include HCoV-229E, HCoV-NL63, HCoV-OC43, and HCoV-HKU1.

Based on its nucleotide sequence, SARS-CoV-2 appears to be a member of the betacoronaviruses, alongside SARS-CoV and MERS-CoV [2]. Of the six human coronaviruses discovered prior to SARS-CoV-2, SARS-CoV and MERS-CoV were the most deadly and aggressive, with the National Institute of Allergy and Infectious Diseases reporting that SARS-CoV has caused 774 deaths and over 8000 cases and that MERS-CoV has caused 866 deaths and 2519 cases worldwide [3]. This puts the projected mortality rate of both of these viruses at approximately 9.7% and 35.25% respectively. As SARS-CoV-2 continues to spread among the human population, it is imperative to find methods to treat or minimize the severity of the virus to avoid further infection and death.

The large positive-stranded RNA genome of coronaviruses, which ranges in length from 26–32kb, encodes for several structural proteins, including the spike glycoprotein (S), the envelope (E), the nucleocapsid (N) and membrane (M) protein, as well as two poly proteins, pp1a and pp1b [4]. These poly proteins are processed by viral proteases to generate 15 to 16 non-structural proteins (nsps) [5]. One of these proteins, nsp12, is an RNA-dependent RNA polymerase (RdRp), a crucial enzyme in the replication of the RNA viruses.

RdRps facilitate viral replication by acting as the catalytic subunit of the viral replicase [6]. All RdRps consist of a palm, fingers, and thumb subdomain [7]. Of these domains, the palm domain functions as the catalytic core of the polymerase and is composed of four highly conserved domains among all polymerases (A–D) and one domain (E) unique to RNA polymerases [8]. The interactions between the fingers and thumb domains accommodate RNA binding and the initiation, elongation, and termination of RNA synthesis [7,9]. One notable feature of RdRps among coronaviruses is the absence of a hydrophobic pocket located near the palm-thumb subdomain interface. The absence of a hydrophobic pocket in the beta corona viruses limits the effectiveness of non-nucleoside inhibitors that have previously been shown to have inhibitory effects against HIV-1 and hepatitis C [7]. However, this does not diminish the potential of coronavirus RdRp inhibition as a therapeutic treatment; nucleoside inhibitors and other drugs remain potential effective inhibitors against the RdRps of coronaviruses.

The necessity of RdRps for viral replication has made them lucrative viral targets that have shown effectiveness in the treatment of other viruses. For example, in Zika, a flavivirus, RdRp inhibitors were found to inhibit viral replication in a dose-dependent manner [10]. RdRp inhibitors were also shown to be effective in inhibiting replication of another flavivirus, the hepatitis C virus (HCV) [11]. Importantly, aurintricarboxylic acid, an inhibitor of RdRp, was found to inhibit replication of SARS-CoV, a coronavirus that is similar in structure to SARS-CoV-2, more than 1000-fold [12]. A wide variety of studies show that RdRp inhibition has great promise to limit viral replication and infection over a wide range of RNA viruses [10–27]. While many compounds have been theoretically identified as potential inhibitors of the RdRp from SARS-CoV-2 [28–30; Table 1], no effective inhibitor has yet been discovered for the RdRp of SARS-CoV-2. Our study used pharmacophore modeling to identify FDA-approved drugs that have potential to inhibit the RdRp of SARS-CoV-2 to determine future treatment options for infections by this virus.

Table 1: Previously Identified Potential Inhibitors of the RdRp of SARS-CoV-2.

Drug Name	FDA-Approval	Binding Energy (kcal/mol)	Source
Ribavirin	FDA-Approved	−7.8	[28]
Remdesivir	FDA-Approved	−7.6	[28]
Sofosbuvir	FDA-Approved	−7.5	[28]
Galidesivir	FDA-Approved	−7.0	[28]
Tenofovir	FDA-Approved	−6.9	[28]
GTP	Not FDA-Approved	−8.7	[28]
IDX-184	Not FDA-Approved	−9.0	[28]
Setrobuvir	Not FDA-Approved	−9.3	[28]
YAK	Not FDA-Approved	−8.4	[28]
Saquinavir	FDA-Approved	−7.8	[29]
Tipranavir	FDA-Approved	−7.8	[29]
Olysio	FDA-Approved	−8.3	[29]
Lonafarnib	Not FDA-Approved	−8.4	[29]
Cepharanthine	Not FDA-Approved	−7.9	[29]
Tegobuvir	Not FDA-Approved	−8.2	[29]
Filibuvir	Not FDA-Approved	−7.7	[29]
Valganciclovir	FDA-approved	N/A	[30]
Chlorhexidine	FDA-approved	N/A	[30]
Ceftibuten	FDA-approved	N/A	[30]
Fenoterol	FDA-approved	N/A	[30]
Fludarabine	FDA-approved	N/A	[30]
Itraconazole	FDA-approved	N/A	[30]
Cefuroxime	FDA-approved	N/A	[30
Atovaquone	FDA-approved	N/A	[30]
Chenodeoxycholic acid	FDA-approved	N/A	[30]
Cromolyn	FDA-approved	N/A	[30]
Pancuronium bromide	FDA-approved	N/A	[30]
Cortisone	FDA-approved	N/A	[30]
Tibolone	FDA-approved	N/A	[28]
Novobiocin	FDA-approved	N/A	[30]
Silybin	FDA-approved	N/A	[30]
Idarubicin	FDA-approved	N/A	[30]
Bromocriptine	FDA-approved	N/A	[30]
Diphenoxylate	FDA-approved	N/A	[30]
Benzylpenicilloyl G	FDA-approved	N/A	[30]
Dabigatran etexilate	FDA-approved	N/A	[30]

Methods

Pharmacophore design and use

To generate a pharmacophore model, we began by identifying possible interactions between the RdRp–nsp7–nsp8 complex and the triphosphate form of remdesivir (PDB ID: 7BV2), an investigational antiviral drug that represents a potential inhibitor of RdRP and has been shown to improve recovery time in SARS-CoV-2-infected patients [30,31]. While the 2.5 Å resolution of this structure is not ideal from our experience, it is sufficient

for pharmacophore-based modeling. We then constructed a pharmacophore model of 11 different features with Molecular Operating Environment (MOE; CCG, Montreal, Canada) based on these possible interactions. These features include two acceptors, three donors, one acceptor and donor, three donor or acceptor, and one hydrophobic; an excluded volume of R=1.1 Å was added. Excluded volume is a spatial constraint imposed on selected atoms of the ligand molecule; it prevents intersection of ligand with inactive protein's atoms. Using this pharmacophore model, we ran a pharmacophore search on our conformational database (DB) of approximately 2500 FDA-approved drugs and 600 000 conformations to identify potential drug-candidates. Based on the results of multiple searches to determine the optimal number of features to use in a partial search that maximized the number of potential drug-candidates without making the pharmacophore model too unrestrictive, we found that a partial search including 6 of the 11 features yielded 315 different compounds and 26 398 conformations. Of these compounds, 85 were chosen based on the number of H-bonds and hydrophobic interactions in the best docking pose.

To find the same-type structures with similar properties and functions, we clustered these compounds, using the Jarvis-Patrick clustering method implemented in MOE under Fingerprint/ Clusters application. A Fingerprint was set to a Graph 3-Point Pharmacophore (Gpi-DAPH3). The Tanimoto coefficient was applied with both similarity threshold S and overlap threshold O both set to 45%. To illustrate the possible structural similarity of compounds in the obtained clusters, we conducted flexible alignments of compounds in each cluster.

Docking of drug conformers

To define the putative best binding drugs, we conducted docking of multiple conformers of the drugs selected from a pharmacophore-based search and of random compounds to the binding site of SARS-CoV-2 RdRp. For docking the selected compounds, we used the same crystal structure of RdRp as earlier (PDB ID: 7BV2). Docking of the selected compounds was done using AutoDock Vina, an open-source program for doing molecular docking (http://vina.scripps.edu/), and conformers of each of the selected compounds were generated using Open Babel (http://openbabel.org). However, since AutoDock Vina does not support docking compounds with certain atoms such as Gadolinium, compounds like Gadobenate were not used. Random control compounds were selected, using a random number generator (https://www.calculator.net/random-number-generator.html) by a 100-compound, simple-random subset without replacing of the entire ZINC 15 database compounds. Compounds with molecular weight less than 300 g/mol were substituted with larger ones. In addition, compounds that were found in the selected FDA-approved drugs list were replaced. Selected random compounds were docked with RdRp in the same processes as selected FDA-approved drugs. The conformers of the compound with ID: ZINC001779539170 had their silicon atom replaced with carbon due to AutoDock Vina's restraints regarding supported atoms.

Based on the docked position of ligands in 7BV2, an RdRp pocket site was defined, which included the following residues: Ala547, Lys545, Arg553, Val557, Cys622, Asp623, Thr680, Ser682, Thr687, Asn691, Asp760 and Asp761.

The Comet supercomputing system

SDSC's Comet supercomputer is an NSF funded cluster (NSF grant: ACI #1341698) that was integrated by Dell. The system features 1944 standard compute nodes with Intel E5-2680v3 (Haswell) processors, 72 GPU nodes (NVIDIA K80, P100 GPUs), and four large memory (1.5 TB) nodes [32]. The nodes are interconnected using a high performance Mellanox fourteen data rate (FDR) InfiniBand network and share two Lustre parallel file systems (hardware from Aeon Computing). All the computations for this paper were conducted on the standard compute nodes that have 24 cores (12 per socket), 128 GB DDR4 DRAM (64 GB per socket), and 320 GB of solid-state drive (SSD) local scratch memory.

File conversion and docking workflow

The computational workflow involves conversion of pdb files of drug conformers into the pdbqt format, scripts that use Comet's node local SSD storage to bundle the tasks involving docking of drug conformers using the AutoDock Vina software, and extraction of mode one energies from the output. The individual docking computations are conducted using 8 cores based on the parallelism possible with the constraint of the exhaustiveness parameter (set to 8 for the analysis). The details of the workflow are provided in [33].

Results

Among the compounds selected by the pharmacophore search of the FDA-approved drug Database, we identified 85 compounds that were separated by similarity–overlap of compounds' three-point pharmacophore graphs into clusters AK. The two largest clusters, clusters A and B, contain 21 and 11 compounds respectively; clusters C, D, and E contain 8, 4, and 3 compounds correspondingly; 6 clusters (F–K) contain 2 compounds, and 26 compounds are not clustered. Compounds in clusters A–E are listed in Table 2 and other compounds can be found in Supplemental Materials (Table S1). Flexible alignment of clusters A–D was used to illustrate compounds' common features (Figures 1 and 2). Cluster A contains mainly cephalosporin antibiotics that bind to the penicillin binding proteins of bacteria, Cluster B contains mainly tetracycline-like antibiotics that bind to ribosomal bacterial proteins, and cluster C contains mainly aminoglycoside antibiotics that also bind to ribosomal bacterial proteins. Cluster D contains two protease inhibitors, a fluoroquinolone antibiotic, and a cholecystokinetic drug, and Cluster E contains two topical drugs used to treat ocular hypertension and the 6-alpha-hydroxy acid form of a cholesterol-lowering medication known as statin.

Next, we compared the docking results for the selected drug compounds with the docking results of random compounds to evaluate the area of significance in the values of binding energies

Table 2: Clusters of the selected by pharmacophore search drugs.

Cluster				
A	**B**	**C**	**D**	**E**
Cefadroxil	Chlortetracycline	Amikacin	Alatrofloxacin	Latanoprost
Cefamandole	Demeclocycline	Azithromycin	Asunaprevir	Pravastatin
Cefdinir	Lymecycline	Framycetin	Ritonavir	Travoprost
Cefmenoxime	Methacycline	Gentamicin	Sincalide	
Cefmetazole	Minocycline	Kanamycin		
Cefoperazone	Omadacycline	Netilmicin		
Cefotaxime	Oxytetracycline	Streptomycin		
Cefotetan	Rolitetracycline	Tobramycin		
Cefoxitin	Sarecycline			
Cefpiramide	Tetracycline			
Cefprozil	Tigecycline			
Ceftibuten				
Ceftobiprole				
Ceftolozane				
Cephalexin				
Cephaloglycin				
Cephalothin				
Folic Acid				
Methotrexate				
Pemetrexed				
Pralatrexate				

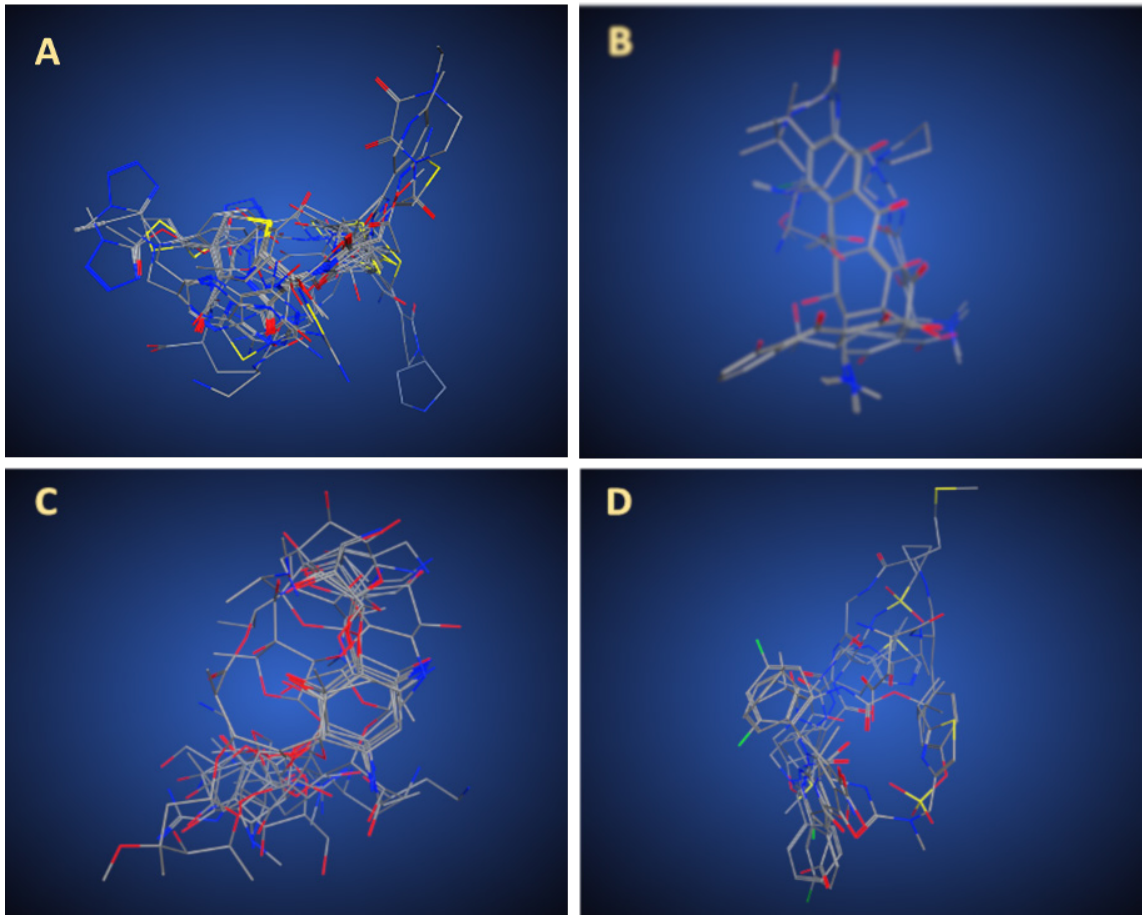

Figure 1: Flexible alignment of the predicted drug candidates: (A) cluster A, (B) cluster B, (C) cluster C, (D) cluster D.

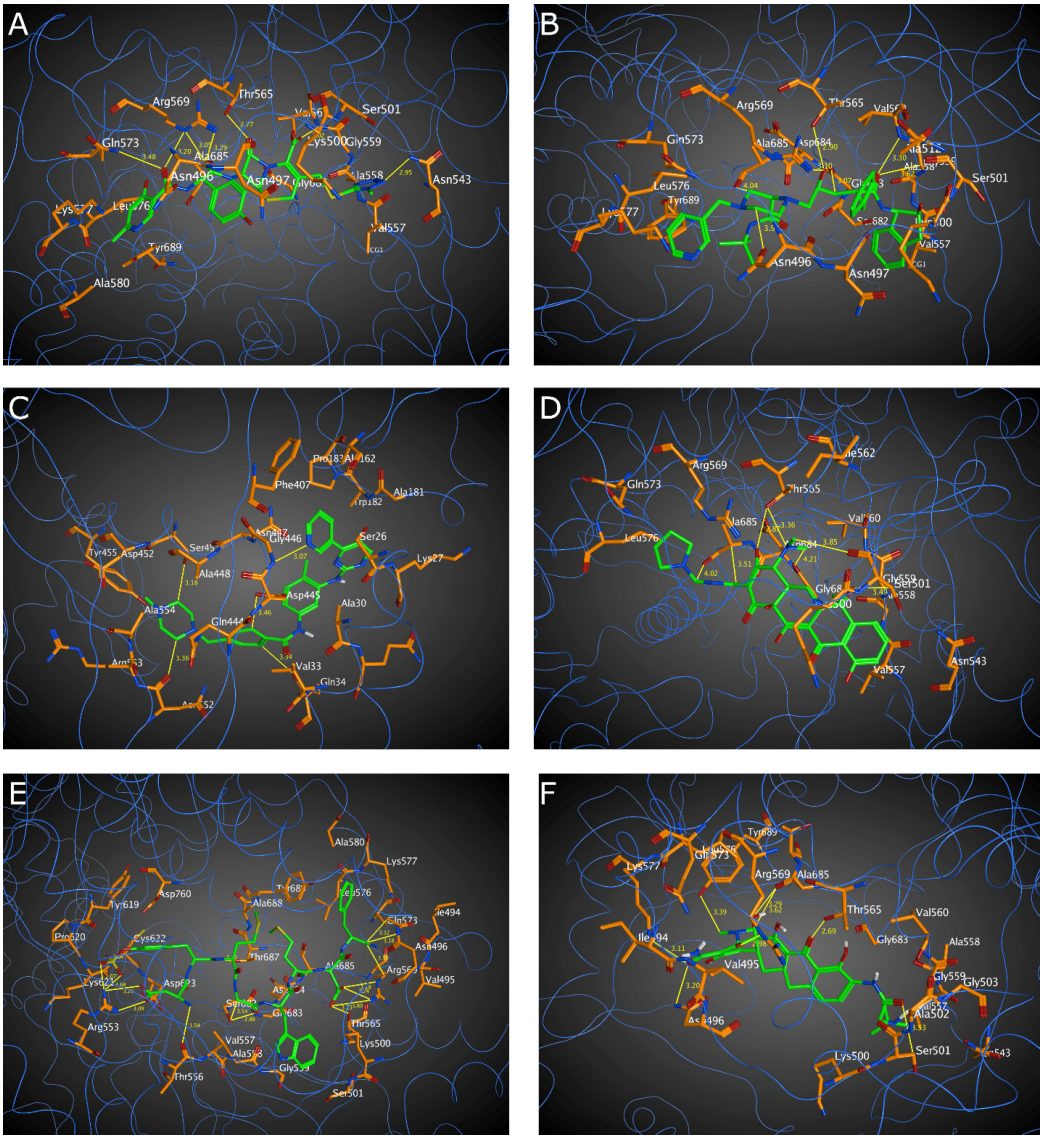

Figure 2: Binding position of the drugs with the best scores in RdRp: (A) Cefpiramide, docking free energy (DFE) = −8.9 kcal/mol. (B) Indinavir, DFE = −9.0 kcal/mol. (C) Imatinib, DFE = −9.2 kcal/mol. (D) Rolitetracycline DFE = −9.0 kcal/mol. (E) Sincalide, DFE = −9.3 kcal/mol. (F) Tigecycline, DFE = −9.2 kcal/mol.

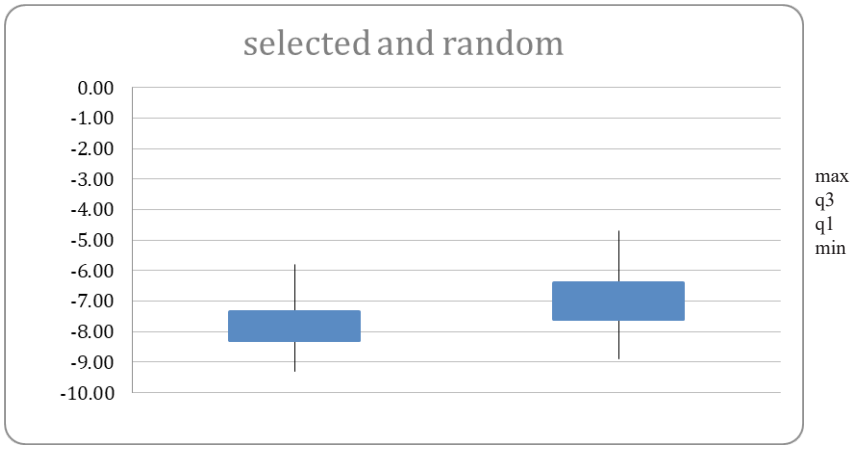

Figure 3: Free energies of docking interactions of selected (left) and random (right) compounds with RdRp. The vertical black lines indicate the full range of binding energies, while the blue boxes indicate the interquartile range. The legend to the right (max, q3, q1 and min) indicates the maximum, third quartile, first quartile, and minimum respectively.

Table 3: List of top energies docked compounds sorted by their energies of interaction with COVID-19 RdRp in the docked positions.

Drug	Energy*	Cluster	Drug	Energy*	Cluster
Sincalide	−9.3	D	Cefmenoxime	−7.9	A
Imatinib	−9.2	I	Cefoxitin	−7.9	A
Tigecycline	−9.2	B	Chlortetracycline	−7.9	B
Indinavir	−9.0	S	Sarecycline	−7.9	B
Rolitetracycline	−9.0	B	Amikacin	−7.8	C
Cefpiramide	−8.9	A	Cefamandole	−7.8	A
Methotrexate	−8.9	A	Kanamycin	−7.8	C
Ceftobiprole	−8.9	A	Udenafil	−7.8	S
Ceftolozane	−8.7	A	Riboflavin	−7.7	S
Alatrofloxacin	−8.7	D	Gentamicin	−7.7	C
Cefoperazone	−8.7	A	Amprenavir	−7.7	K
Cefotetan	−8.7	A	Ceftibuten	−7.7	A
Dasatinib	−8.7	I	Cephaloglycin	−7.7	A
Azithromycin	−8.7	C	Framycetin	−7.7	S
Omadacycline	−8.6	B	Lenvatinib	−7.7	S
Daunorubicin	−8.5	J	Minocycline	−7.7	B
Ritonavir	−8.4	D	Regadenoson	−7.7	H
Asunaprevir	−8.3	D	Cefadroxil	−7.6	A
Lymecycline	−8.3	B	Oxytetracycline	−7.6	B
Streptomycin	−8.3	C	Tetracycline	−7.6	B
Doripenem	−8.3	G	Tobramycin	−7.6	C
Pralatrexate	−8.3	A	Travoprost	−7.6	E
Rutin	−8.3	J	Adefovir	−7.6	F
Chlorohexidine	−8.2	S	Demeclocycline	−7.5	B
Ertapenem	−8.2	G	Cephalexin	−7.4	A
Phthalylsulfathiazole	−8.2	S	Netilmicin	−7.4	C
Folic acid	−8.2	A	Ranolazine	−7.3	S
Sofosbuvir	−8.1	S	Cefdinir	−7.3	A
Glimepiride	−8.1	S	Cefotaxime	−7.2	A
Hydrocortamate	−8.1	S	Fosamprenavir	−7.1	K
Ximelagatran	−8.0	S	Cefprozil	−7.1	A
Capecitabine	−8.0	S	Ixazomib	−7.1	S
Eprosartan	−8.0	S	Pravastatin	−7.0	E
Methacycline	−8.0	B	Dipyridamole	−7.0	S
Pemetrexed	−8.0	A	Peramivir	−7.0	S
Bosentan	−7.9	H			

*Docking free energy; S—single compound cluster

(Figure 3). It is important to note is that since pharmacophore-based selection is such a powerful tool, drugs with binding energies on the same level of the random compounds do not have to be completely discarded. The binding energies of the selected compounds can be found in Table 3. Note that drugs from clusters A, B, and D are at the top of the table and that often the binding positions of real drugs seen in crystal structures are not in the poses calculated to be the minimal docking energy positions.

Discussion

Based on the crystal structure of SARS-CoV-2 RdRp (PDB ID: 7BV2), we developed a pharmacophore model of the binding pocket of this protein. Using this model, we browsed our conformational database of FDA-approved drugs and obtained 85 compounds that were clusterized for selecting the most promising candidates based on their pharmacophores 3D profiles. We then conducted multi conformational docking of the selected compounds to the RdRp pocket. The drug list obtained with pharmacophore search includes several drugs that were shown to be effective against 19 viruses including ZIKV, HCV, MERS-CoV, SARS-CoV, SARS-CoV-2, and others (Figure 4). All except BK Virus are ssRNA viruses, although the potential role of these compounds as inhibitors of RdRp remains to be evaluated.

We are aware of three other studies where docking experiments were used to predict binding of existing pharmaceuticals to the SARS-CoV-2 RdRp [28–30]. All prior studies relied on homology modeling to construct 3D structures of RdRp. Wu et al. [30] studied 2924 compounds from ZINC Drug Database; Ruan et al. [29] studied 7496 FDA-approved, world-not-FDA, and investigational-only compounds from the ZINC Drug database; Elfiky [28] studied several known anti-polymerase drugs. Two compounds were identified in the present study by either Wu et al. [30] or Elfiky [28]: ceftibuten and sofosbuvir. The remaining compounds identified here are unique to our study. This may reflect the influence of using the crystal structure of SARS-CoV-2 as the

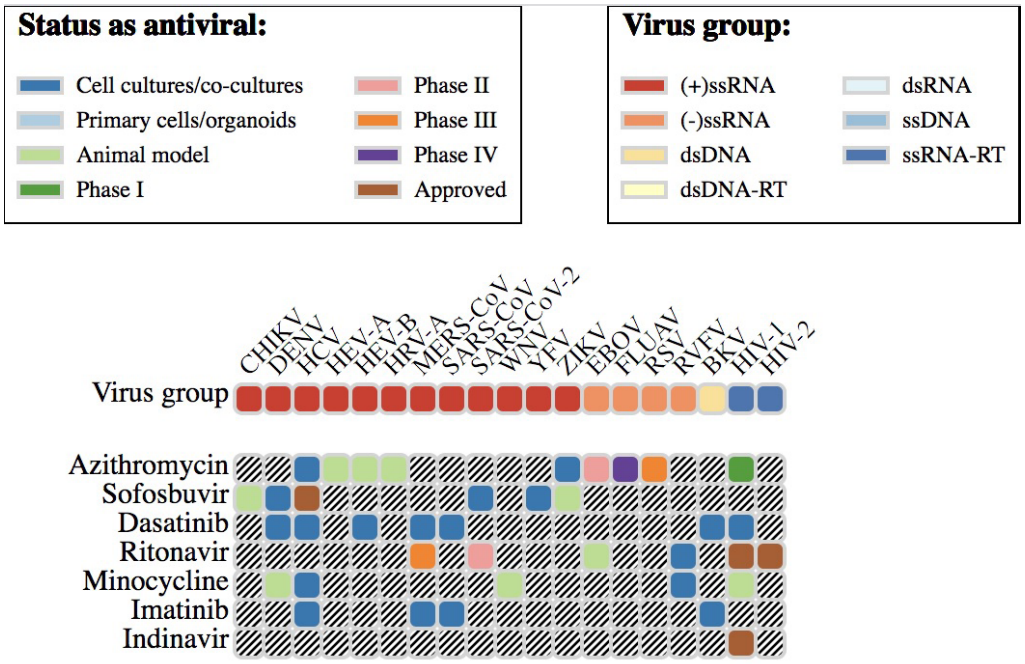

Figure 4: A chart representing known seven of the selected compounds and their effectiveness against different viruses.

starting point in the present study, and a difference in methodology in our case including preliminary pharmacophore-based search before docking computational experiments.

Seven of the compounds selected by our computations have been experimentally tested for activity against several viruses according to the DrugVirus.info database [34]: azithromycin was effective against HEV-A, HEV-B, and HRV-A in animal models and is currently undergoing clinical trials against EBOV, FLUAV, RSV, and HIV-1; dasatinib was active against DENV, HCV, HEV-B, MERS-CoV, SARS-CoV, BKV, and HIV-1 in cell culture assays; sofosbuvir was approved to be used against HCV and was effective against CHIKV, DENV, SARS-CoV-2, YFV, and ZIKV; minocycline was tested and proven active against DENV, HCV, WNV, RVFV, and HIV-1; imatinib has been confirmed to be active against HCV, MERS-CoV, SARS-CoV, and BKV *in vitro*; ritonavir was approved to be used against HIV-1 and HIV-2 and is currently undergoing phase III clinical trials against MERS-CoV and phase II for SARS-CoV-2. The docking energies of these drugs were −8.7 kcal/mol for azithromycin, −8.7 kcal/mol for dasatinib, −8.1 kcal/mol for sofosbuvir, −7.7 kcal/mol for minocycline, −9.2 kcal/mol for imatinib, and −8.4 kcal/mol for ritonavir. While the majority of experimental testing was done in cell-cultures, a significant number of these drugs are active in animal models and two are FDA approved for the treatment of other viruses. The computational studies previously mentioned [28–30] only identified one of these six compounds (sofosbuvir) as a potential inhibitor of SARS-CoV-2 RdRp [28]. However, Wu et al. [30] identified three other compounds, itraconzole, tenofovir, and atovaquone that this study did not identify and Elfiky [28] identified three different compounds, remdesivir, galidesivir, and ribavirin that this study also did not identify. Differences in methodology, specifically the utilization of a pharmacophore model present in this study, may explain these differences. Additionally, several of these drugs such as remdesivir, galidesivir, and tenofovir are not approved by the FDA, meaning that they were not included in the database that was initially searched for compounds and thus could not be identified by our model.

It is interesting to note that four of these six compounds were found to be effective against HCV in culture and that one of the drugs has been approved by the FDA against HCV. After performing a pairwise sequence alignment using EMBOSS Needle of SARS-CoV-2 RdRp and HCV RdRp under the assumption that their similar function might be the cause of the similarities in the drugs active against them, we discovered that while the sequences themselves are not similar in terms of percent identity of 8.1%, 4 of the 12 residues that we included in our pharmacophore model of the binding site, ASP623, THR680, ASP760, and ASP761, were conserved in the 3D overlay with HCV and one residue, ASN691, was hydrophilic in both proteins with the corresponding residue of HCV being ASP232. Considering that our pharmacophore query searched for compounds that matched 6 of the 11 features that we included in our pharmacophore model, the fact that 5 main residues have similar properties between SARS-CoV-2 and HCV could explain why five of the six compounds identified here as potential inhibitors of SARS-CoV-2 RdRp are effective in some way against HCV.

Given the severity of the SARS-CoV-2 pandemic and the lack of treatment options available against the virus, the identification of FDA-approved drugs that could be utilized against SARS-CoV-2 has the potential to lead to advances in the treatment of the virus. While this study is limited because it utilizes only computer-based

screening to identify potential treatments instead of either *in vitro* or *in vivo* testing, identifying 85 FDA-approved compounds that could limit the viral replication of SARS-CoV-2 is an important step that could lead to clinical trials and eventually treatments that could alleviate the effects of this virus.

Acknowledgements

We would like to thank the people of San Diego Supercomputer Center and CCG (Montreal, Canada) and personally Guillaume Fortin for friendly support.

Funding: The SDSC Comet supercomputer is supported by the NSF grant: ACI #1341698 Gateways to Discovery: Cyber infrastructure for the Long Tail of Science. MAM was supported by NIH R01 GM126463.

Author contributions: IFT and VLK introduced initial idea of the project; VLK and CK conducted pharmacophore development, databases searches, clustering and multiconfromational alignment; MAM, IFT, and VLK conducted interpretation of the results; AZ and MT conducted computational docking on Comet supercomputer; IFT, VLK, CK, MAM, and AZ wrote the article.

References

1. https://gisanddata.maps.arcgis.com/apps/opsdashboard/index.html#/bda7594740fd40299423467b48e9ecf6
2. Jaimes JA, André NM, Chappie JS, et al. Phylogenetic analysis and structural modeling of SARS-CoV-2 spike protein reveals an evolutionary distinct and proteolytically sensitive activation loop. J Mol Biol. 2020; 432: 3309-3325.
3. https://www.niaid.nih.gov/diseases-conditions/COVID-19
4. Bartlam M, Yang H, Rao Z. Structural insights into SARS coronavirus proteins. Curr Opin Struct Biol. 2005; 15: 664-672.
5. Tan Y-J, Lim SG, Hong W. Characterization of viral proteins encoded by the SARS-coronavirus genome. Antiviral Res. 2005; 65: 69-78.
6. O'Reilly EK, Koo CC. Analysis of RNA-dependent RNA polymerase structure and function as guided by known polymerase structures and computer predictions of secondary structure. Virology. 1998; 252: 287-303.
7. Xu X, Liu Y, Weiss S, et al. Molecular model of SARS coronavirus polymerase: Implications for biochemical functions and drug design. Nucleic Acids Res. 2003; 31: 7117-7130.
8. Poch O, Sauvaget I, Delarue M, et al. Identification of four conserved motifs among the RNA-dependent polymerase encoding elements. EMBO J. 1989; 8: 3867-3874.
9. Butcher SJ, Grimes JM, Makeyev EV, et al. A mechanism for initiating RNA-dependent RNA polymerization. Nature. 2001; 410: 235-240.
10. Sacramento CQ, de Melo GR, de Freitas CS, et al. The clinically approved antiviral drug sofosbuvir inhibits Zika virus replication. Sci Rep. 2017; 7: 40920.
11. Deore RR, Chern JW. NS5B RNA dependent RNA polymerase inhibitors: The promising approach to treat hepatitis C virus infections. Curr Med Chem. 2010; 17: 3806-3826.
12. Yap Y, Zhang X, Andonov A, et al. Structural analysis of inhibition mechanisms of aurintricarboxylic acid on SARS-CoV polymerase and other proteins. Comput Biol Chem. 2005; 29: 212-209.
13. Graham RL, Sparks JS, Eckerle LD, et al. SARS coronavirus replicase proteins in pathogenesis. Virus Res. 2008; 133: 88-100.
14. Niyomrattanakit P, Chen Y-L, Dong H, et al. Inhibition of dengue virus polymerase by blocking of the RNA tunnel. J Virol. 2010; 84: 5678-5686.
15. Wu Y-C, Lu Y-F, Chi S-C. Anti-viral mechanism of barramundi Mx against betanodavirus involves the inhibition of viral RNA synthesis through the interference of RdRp. Fish Shellfish Immunol. 2010; 28: 467-775.
16. Dhanak D, Duffy KJ, Johnston VK, et al. Identification and biological characterization of heterocyclic inhibitors of the hepatitis C virus RNA-dependent RNA polymerase. J Biol Chem. 2002; 277: 38322-38327.
17. Ahmed-Belkacem A, Ahnou N, Barbotte L, et al. Silibinin and related compounds are direct inhibitors of hepatitis C virus RNA-dependent RNA polymerase. Gastroenterology. 2010; 138: 1112-1122.
18. Yao X, Guo S, Wu W, et al. Q63, a novel DENV2 RdRp non-nucleoside inhibitor, inhibited DENV2 replication and infection. J Pharmacol Sci. 2018; 138: 247-256.
19. Ma J, Wang,W, Zeng L, et al. Inhibition of the replication of grass carp reovirus in CIK cells with plasmid-transcribed shRNAs. J Virol Methods. 2011; 175: 182-187.
20. Hung H-C, Chen T-C, Fang M-Y, et al. Inhibition of enterovirus 71 replication and the viral 3D polymerase by aurintricarboxylic acid. J Antimicrob Chemother. 2010; 65: 676¬683.
21. Pelliccia S, Wu YH, Coluccia A, et al. Inhibition of dengue virus replication by novel inhibitors of RNA-dependent RNA polymerase and protease activities. J Enzyme Inhib Med Chem. 2017; 32: 1091-1101.
22. Pattnaik A, Palermo N, Sahoo BR, et al. Discovery of a non-nucleoside RNA polymerase inhibitor for blocking Zika virus replication through in silico screening. Antiviral Res. 2018; 151: 78¬86.
23. Huang F, Hua X, Yang S, et al. Effective inhibition of hepatitis E virus replication in A549 cells and piglets by RNA interference (RNAi) targeting RNA-dependent RNA polymerase. Antiviral Res. 2009; 83: 274-281.
24. Yoo J-S, Kim C-M, Kim J-H, et al. Inhibition of Japanese encephalitis virus replication by peptide nucleic acids targeting cis-acting elements on the plus- and minus-strands of viral RNA. Antiviral Res. 2009; 82: 122-133.
25. Boonrod K, Galetzka D, Nagy PD, et al. Single-chain antibodies against a plant viral RNA-dependent RNA polymerase confer virus resistance. Nat Biotechnol. 2004; 22: 856-862.
26. Castro EF, Fabian LE, Caputto ME, et al. Inhibition of bovine

viral diarrhea virus RNA Synthesis by thiosemicarbazone derived from 5, 6-dimethoxy-1-indanone. J Virol. 2011; 85: 5436-5445.

27. Yuan J, Yu J, Huang Y, et al. Antibiotic fidaxomicin is an RdRp inhibitor as a potential new therapeutic agent against Zika virus. BMC Med. 2020; 18: 204.
28. Elfiky AA. Ribavirin, Remdesivir, Sofosbuvir, Galidesivir, and Tenofovir against SARS-CoV-2 RNA dependent RNA polymerase (RdRp): A molecular docking study. Life Sci. 2020; 253: 117592.
29. Ruan Z, Liu C, Guo Y, et al. Potential inhibitors targeting RNA-dependent RNA polymerase activity (NSP12) of SARS-CoV-2. J Med Virol. 2020; 10.1002/jmv.26222.
30. Wu C, Liu Y, Yang Y, et al. Analysis of therapeutic targets for SARS-CoV-2 and discovery of potential drugs by computational methods. Acta Pharm Sin B. 2020; 10: 766-788.
31. Mahase E. COVID-19: Remdesivir is helpful but not a wonder drug, say researchers. BMJ (Clinical research ed.). 2020; 369.
32. Moore RL, Baru C, Baxter D, et al. Gateways to discovery: Cyberinfrastructure for the long tail of science. XSEDE '14: Proceedings of the 2014 Annual Conference on Extreme Science and Engineering Discovery Environment. Association for Computing Machinery: New York, NY, USA. 2014; 39: 1-8.
33. Kouznetsova VL, Zhang A, Tatineni M, et al. Potential COVID-19 papain-like protease PLpro inhibitors: Repurposing FDA-approved drugs. PeerJ: Phys Chem. 2020.
34. Andersen PI, Ianevski A, Lysvand H, et al. Discovery and development of safe-in-man broad-spectrum antiviral agents. Int J Infect Dis. 2020; 93: 268-276.